Generating Order in Gyroid Terpolymer Films During Solvent Vapor Annealing

James A. Dolan,[†,‡,¶] Karolina Korzeb,[§] Raphael Dehmel,[‡,∥] Bodo D. Wilts,[§] Karl C. Gödel,[‡] Morgan Stefik,[⊥] Ulrich Wiesner,[#] Timothy D. Wilkinson,[†] Jeremy J. Baumberg,[‡] Ullrich Steiner,[§] and Ilja Gunkel[*,§]

†*Department of Engineering, University of Cambridge, J.J. Thomson Avenue, Cambridge CB3 0FA, UK*

‡*Department of Physics, University of Cambridge, J.J. Thomson Avenue, Cambridge CB3 0HE, UK*

¶*Current Address: Institute for Molecular Engineering, Argonne National Laboratory, 9700 S. Cass Avenue, Argonne, IL 60439, USA*

§*Adolphe Merkle Institute, Chemin des Verdiers 4, 1700 Fribourg, Switzerland*

∥*Current Address: Papierfabrik Louisenthal GmbH, 83701 Gmund a.T. Germany*

⊥*Department of Chemistry and Biochemistry, University of South Carolina, 541 Main St, Horizon I BLDG, Columbia, SC 29208, USA*

#*Department of Materials Science and Engineering, Cornell University, 214 Bard Hall, Ithaca, NY 14853-1501, USA*

E-mail: ilja.gunkel@unifr.ch

Phone: +41 (0)26 300 73 98

Abstract

Solvent vapor annealing (SVA) is an excellent means to anneal block copolymer thin films, thereby controlling the self-assembly processes from molecular to macroscopic length scales. Triblock terpolymers are excellent candidate materials to generate ordered 3D continuous interpenetrating network morphologies, particularly the gyroid phases, which form over a much wider composition range compared to diblock copolymers. Here, we present the results of *in situ* grazing-incidence small-angle X-ray scattering (GISAXS) experiments on a gyroid-forming triblock terpolymer, polyisoprene-*b*-polystyrene-*b*-poly(ethylene oxide) (ISO), revealing the effects of several key SVA parameters on the morphology, lateral order and, particularly, its preservation in the dried film. The robustness of the terpolymer gyroid morphology is a key requirements for successful SVA, allowing the exploration of annealing parameters which may enable the generation of films with long-range order, e.g. for optical metamaterial applications.

Introduction

Block copolymer (BCP) self-assembly is a particularly promising route to fabricate functional nanomaterials over macroscopically large areas.[1] For many applications, long-range order on the millimeter length scale is required, e.g. for one- and two-dimensional (2D) nanolithographic templates[2–4] and three-dimensional (3D) optical metamaterials.[5,6] To produce BCP films with such high degrees of order, it is often advantageous to utilize solvent vapor annealing (SVA). Compared to thermal annealing, the introduction of controlled amounts of a suitable solvent greatly increases the mobility of the BCP, thereby reducing the timescale of self-assembly. By carefully tuning solvent extraction, it is possible to substantially increase the resulting size of the self-assembled grains.[7–10]

The effect of SVA on linear diblock copolymers is well understood.[11,12] In the ideal case of a non-selective good solvent, both blocks of the copolymer swell equally, leaving the effective volume fractions of the blocks f_{A} and f_{B} unaltered, but screening the interaction between the two blocks (i.e. lowering the Flory-Huggins interaction parameter χ_{AB}). A sufficiently high solvent concentration lowers χ_{AB} to such an extent that the microphase-separated morphology is no longer thermodynamically favorable and the copolymer forms a disordered phase. A selective solvent, on the other hand, preferentially swells one of the blocks, altering the effective volume fractions and thereby influencing the equilibrium morphology of the swollen copolymer.[13–15] It is thus possible to explore the entire phase space of diblock copolymers (i.e. spheres, cylinders, the double gyroid and lamellae) with only a single copolymer by varying the solvent concentration and selectivity.[14]

When using diblock copolymers, the double gyroid morphology forms only in a relatively small composition ratio of the two blocks, which makes the control of grain growth difficult because of the sensitivity with respect to undesired morphological transitions. This hinders efforts to improve the long-range order in the only 3D interconnected diblock copolymer morphology, i.e. the double gyroid. She *et al.* demonstrated the controlled ordering of the double gyroid morphology in diblock copolymer thin films upon annealing in a neutral solvent

and employing a functionalized substrate.[16] Similarly, Wu *et al.* explored the effect of swollen thickness and solvent removal rate on the resulting morphology of solvent-annealed gyroid-forming diblock copolymers.[17] Both publications report, however, morphological transitions to the cylinder phase, despite the use of a supposedly neutral solvent. Coexisting spherical and gyroid morphologies were also observed, further demonstrating the difficulty of retaining the gyroid phase in diblock copolymer swollen melts during SVA, impeding the improvement of long-range order in this system.[14]

It is well known that triblock terpolymers form 3D interconnected morphologies for much wider block-composition ranges compared to diblock copolymers.[18,19] For example, the double gyroid (Q^{230}) in bulk polyisoprene-*b*-polystyrene (PI-*b*-PS) diblock copolymers forms for $0.36 < f_{\mathrm{PI}} < 0.39$ and $0.65 < f_{\mathrm{PI}} < 0.69$,[20,21] while its core-shell counterpart (also Q^{230}) in bulk polyisoprene-*b*-polystyrene-*b*-poly(ethylene oxide) (ISO) triblock terpolymers forms for $f_{\mathrm{PI}}/f_{\mathrm{PS}} = 1.38, 0.14 < f_{\mathrm{PEO}} < 0.20$ and $f_{\mathrm{PI}}/f_{\mathrm{PS}} = 1.27, 0.11 < f_{\mathrm{PEO}} < 0.20$.[19,22,23] The alternating gyroid (Q^{214}) in bulk ISO terpolymers shows a similarly large composition range: $f_{\mathrm{PI}}/f_{\mathrm{PS}} = 0.64, 0.14 < f_{\mathrm{PEO}} < 0.18$ and $f_{\mathrm{PI}}/f_{\mathrm{PS}} = 0.45, 0.17 < f_{\mathrm{PEO}} < 0.29$.[19,22,23]

For functionalities that benefit from ordered gyroid phases, it is therefore advantageous to induce long-range lateral order by means of SVA in triblock terpolymers rather than diblock copolymers. In this system, it should be possible to maintain the chosen gyroid morphology during solvent uptake even for changes in the volume fractions of the three blocks caused by solvent selectivities. The study of morphological evolution of linear triblock copolymers (ABA) and terpolymers (ABC) during SVA has, however, received relatively little attention, and SVA of gyroid-forming triblock copolymers or terpolymers has not yet been investigated. Previous studies on ABA triblock copolymers focused instead on the morphological transitions resulting from the exposure to selective and neutral solvents,[24] the improvement in symmetry and long-range order of the cylindrical and lamellar microphase-separated morphologies,[24] and the effect of the solvent evaporation rate on the orientation of cylindrical domains.[25–27] Early studies on ABC triblock terpolymer films investigated the

effect of solvent,[28] solvent removal rate,[28,29] and annealing time[30] upon morphology and domain orientation.

In this work, we study the kinetics and thermodynamics of a linear, gyroid-forming ISO triblock terpolymer during SVA using grazing-incidence small-angle X-ray scattering (GISAXS). GISAXS is the most direct means to study the microphase-separated morphology of block copolymers *in situ* during SVA, allowing the simultaneous characterization of both in- and out-of-plane electron density correlations over macroscopically large areas in real time.[8,13–15,31–34] We annealed ISO terpolymer films in the mixed vapors of tetrahydrofuran (THF) and methanol of various compositions, and identified the resulting microphase-separated morphologies and degree of order upon varying the maximum solvent concentration and solvent removal rate.

Methods

Polymer Films. The polyisoprene-*b*-polystyrene-*b*-poly(ethylene oxide) (ISO) triblock terpolymer with a total molecular weight of 33 kg mol^{-1} was prepared by anionic polymerization following synthesis procedures reported elsewhere.[35,36] The block volume fractions of the terpolymer were $f_{\mathrm{PI}} = 0.31$, $f_{\mathrm{PS}} = 0.52$, and $f_{\mathrm{PEO}} = 0.17$. Thin films of the ISO terpolymer were prepared atop silicon substrates which were cleaned by exposure to an oxygen plasma (Diener MRC 100 at 100% power for 2 min). Thin films were spun from a 10% (w/w) solution of ISO terpolymer in anhydrous anisole (Sigma-Aldrich) for 60 s at 1200 rpm with an acceleration of 500 rpm s^{-1}. The resulting film thickness was 520 nm to 560 nm as determined by thin film interferometry (see below).

Polyisoprene (PI), polystryene (PS), and polyethylene oxide (PEO) homopolymer films with number-average molecular weights of 103 kg mol^{-1} (polydispersity of 1.07), 103 kg mol^{-1} (polydispersity of 2.5), and 100 kg mol^{-1}, respectively, were spun atop silicon substrates (cleaned as above) for 60 s at 3200 rpm with an acceleration of 500 rpm s^{-1}. Resulting film

thicknesses were 534 – 551 nm (PI), 750 – 763 nm (PS), and 982 – 996 nm (PEO).

Solvent Vapor Annealing. The samples were exposed to controlled amounts of solvent vapor using a custom-made annealing chamber. The polyetheretherketone (PEEK) annealing chamber had sealed Kapton windows on two opposing sides (for transmission of the incident and scattered X-ray beams) and a sealed quartz glass window in the lid (for measurement of the film thickness during annealing). Three gas lines were joined and the mixed gas flowed into and through the chamber, creating a well-defined solvent atmosphere within it: dry nitrogen flowed through one of the three lines, whilst for the other two the dry nitrogen was bubbled through various solvents. By controlling the volume flow rate in each line with three independently controlled mass flow controllers (MKS Type MF1, flow range 100 sccm, MKS Type 647 multichannel gas flow controller unit), the ratio of solvent-saturated to dry nitrogen (i.e. the "concentration" of the—potentially mixed—solvent vapor) flowing into the chamber was controlled. Custom-built software controlled the flow rates to adjust the desired solvent vapor concentration in the chamber, enabling the implementation of predetermined solvent annealing protocols.

Tetrahydrofuran (THF) and methanol (Sigma-Aldrich) were employed as solvents. Unless otherwise noted, the combined mass flow rate was maintained at 20 sccm throughout the experiments. Upon exiting the chamber, the gas mixture flowed into an exhaust line through a manual mass flow controller which could be adjusted to ensure the maintenance of a sufficiently high solvent vapor pressure in the annealing chamber. The temperature of the sample within the annealing chamber was controlled using a Peltier element mounted on a copper plate, and the solvent reservoirs were immersed in a temperature-controlled water bath (ThermoFisher ARCTIC SC150-A10B Refrigerated Circulator). Unless otherwise noted, the temperature of the solvent was held at ≈ 23.0°C, while the temperature of the sample was varied between $\approx 21.3 - 24.4\,$°C, depending on the required swelling ratio (a lower sample temperature resulting in greater swelling). The temperature of the solvent was

Table 1: Ratios of swollen to dry film thicknesses of ISO terpolymer and corresponding homopolymer films annealed in saturated atmospheres of THF and a THF/methanol mixture (THF:MeOH).

Solvent	**PS**	**PI**	**PEO**	**ISO**
THF	1.37	1.42	1.06	1.36
THF:MeOH (80:20)	1.48	1.36	1.06	1.42

set to a value close to room temperature (≈ 23.7°C) to avoid condensation of solvent in the gas lines. The ambient relative humidity was constant at $\approx 33\%$.

In an attempt to determine the selectivity of THF and methanol mixture vapors for the respective blocks of ISO terpolymer, the swelling behavior of PS, PI, and PEO homopolymer films was characterized by monitoring their relative thickness increase upon exposure to saturated solvent vapor atmospheres (Table 1). The temperature of the samples was kept at $\approx 21\,^{\circ}$C and the relative humidity was $\approx 45-60\%$. PEO did not exhibit any significant swelling regardless of the solvent vapor used, likely related to the semicrystalline nature of homopolymer PEO at room temperature. However, the swelling data for PS and PI reveal a selectivity of THF for PI, and an increasing selectivity of the THF and methonaol mixtures for PS with increasing methanol content.

Film Thickness Measurements. The thickness of the terpolymer films during solvent vapor annealing was measured interferometrically *in situ* using an Avantes AvaLight-DH-S-BAL deuterium halogen light source (only the halogen source, 500 nm – 2500 nm wavelength range) and an Avantes AvaSpec 2048L spectrometer. Light was coupled through a bifurcated optical fiber (FCR-12UV200/600-2-ME) and focused onto the sample *via* a collimator (FCR-COL UV/VIS). The thickness was estimated by assuming a refractive index of $n = 1.5$ for the terpolymer film. The swelling ratio is a dimensionless measure of relative film thickness

and is defined as

$$\varphi = \frac{t}{t_0}, \tag{1}$$

where t is the swollen thickness and t_0 the initial thickness of the as-spun film (i.e. before application of any solvent). Assuming no in-plane motion of the film during annealing, the swelling ratio is the reciprocal of the volume fraction of polymer in the swollen film.

***In Situ* Grazing-Incidence Small-Angle X-Ray Scattering.** GISAXS measurements were performed *in situ* during solvent vapor annealing at the cSAXS beamline of the Swiss Light Source, Paul Scherrer Institute, Villigen, Switzerland. The X-ray energy was 11.2 keV and the sample-to-detector distance was 7232.5 mm, determined by calibration with a silver behenate standard. Scattering patterns were recorded on a PILATUS 2M detector with a 1 s exposure time at angles in the $\alpha_\mathrm{i} = 0.14° - 0.18°$ range. To avoid damaging the terpolymer film by X-ray overexposure, the film was laterally translated by 250 µm prior to each measurement (e.g. after the previous measurement and any alignment protocols).

GISAXS Indexing. Indexing of the 2D GISAXS patterns was performed using the GIXS-GUI software.[37] All GISAXS images were successfully indexed with the reflections of the $I4_132$ space group with the [110] direction oriented perpendicular to the substrate, Miller indices in h, k, l range of -2 to 2, and unit cell parameters in the ranges: 30.8 – 36.2 nm for a and b, 33.3 – 36.0 nm for c, 87.5 – 102° for and γ. The critical angle α_c and the incident angle α_i were varied in the $\alpha_\mathrm{c} = 0.107 - 0.110°$ and $\alpha_\mathrm{i} = 0.173 - 0.179°$ range, respectively.

GISAXS In-Plane Analysis. GISAXS scattering patterns were reduced using *Nika*,[38] a software package for IGOR Pro 6 (WaveMetrics), and the in-plane line integrations were subsequently analyzed using custom software to automatically determine peak locations and widths as a function of the swelling ratio. Peaks [hkl] were analyzed by fitting the composite

function

$$I(q_y) = I_0 + I_1 q_y^{-d} + \sum_{n=1}^{N} \frac{I_{(n)}^{[hkl]}}{1 + \left(\frac{q_y - q_{y(n)}^{[hkl]}}{\Delta q_{y(n)}^{[hkl]}} \right)^2}, \tag{2}$$

to the spectra, where I_0, I_1, d, $I_{(n)}^{[hkl]}$, and $\Delta q_{y(n)}^{[hkl]}$ were varied, and $q_{y(n)}^{[hkl]}$ was fixed during the fitting procedure. Peak positions $q_{y(n)}^{[hkl]}$ were determined prior to fitting by a peak-finding algorithm. The values of the peak widths $\Delta q_{y(n)}^{[hkl]}$ resulted from the fit. Zero ($N = 0$), one ($N = 1$), or two ($N = 2$) Lorentzian peaks were identified during fitting.

Results

To study the kinetics and thermodynamics of the ISO triblock terpolymer during SVA, thin films of the terpolymer were exposed to controlled solvent vapor atmospheres while the resulting film thickness and GISAXS scattering patterns were recorded at regular intervals. SVA "regimes" were identified by tracking the GISAXS scattering patterns and the associated peak metrics (i.e. the position and width) as a function of swelling ratio. The presence and behavior of peaks reveal the effect of the solvent on the film. After swelling the films to a maximum swelling ratio, they were quenched in a nitrogen flow at a well defined quench rate, and the resulting microphase-separated morphology and degree of order in the resulting dried films were investigated. Finally, the effect of the solvent vapor composition—and therefore the varying selectivity of the solvents for the individual blocks of the terpolymer—was similarly studied.

All studied solvent-annealed films exhibited the alternating gyroid microphase-separated morphology. This morphology was assigned based on 2D indexing of the GISAXS scattering patterns (Figure 1). Figure 1(a) shows the successfully indexed GISAXS scattering pattern of an ISO film swollen with the mixed vapors of tetrahydrofuran (THF) and methanol (80:20). The indexed peaks are labeled in Figure 1(b). The peaks observed in the scattering pattern, which is typical for all patterns observed in this study, clearly agree excellently well with the

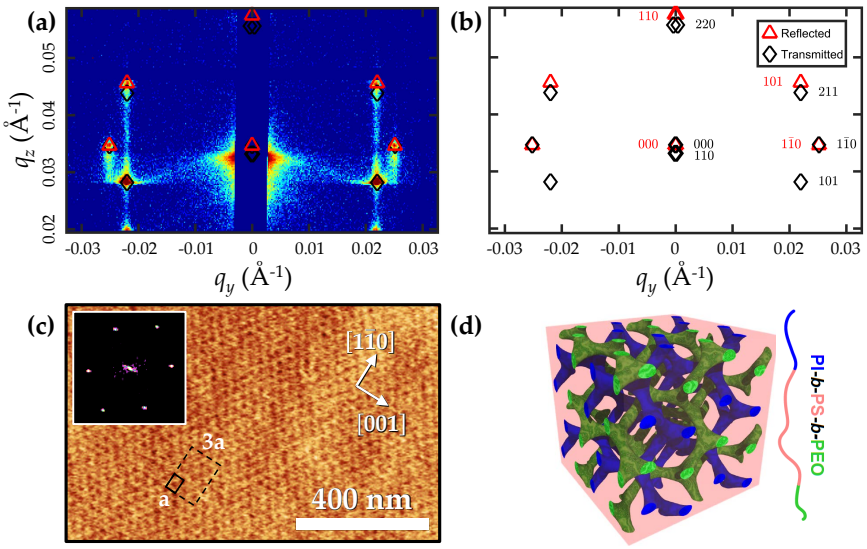

Figure 1: **Alternating gyroid microphase-separated morphology.** The alternating gyroid morphology with the $I4_132$ (single gyroid; Q^{214}) space group was identified in all swollen and dried ISO films. (a) GISAXS scattering pattern of an ISO film swollen in the mixed vapors of THF and methanol (80:20), indexed with first and second order peaks of the $I4_132$ space group with the [110] direction oriented perpendicular to the substrate and the unit cell parameters $a = b = 35.8\,\text{nm}$, $c = 34.9\,\text{nm}$, and $\gamma = 89°$. (b) Corresponding peak labels highlighting the "reflected" (red triangles) and "transmitted" (black diamonds) peak positions.[39] (c) Atomic force microscopy (AFM) amplitude image of the (110) surface of a dried ISO film after annealing in the mixed vapors of THF and methanol (80:20). A unit cell is indicated with a black rectangle. The average periodicity along the [001] and [110] directions (indicated) are 34.5 and 46.2 nm, respectively. They were extracted using the fast Fourier transform (FFT) of the image shown in the inset. (d) Schematic of the alternating gyroid morphology formed by the ISO triblock terpolymer.

expected peaks of the $I4_132$ (single gyroid; Q^{214}) space group, indicative of the alternating gyroid morphology. The [110] direction was oriented perpendicular to the substrate in all studied films. The unit cell parameters ($a = b = 35.8\,\text{nm}$, $c = 34.9\,\text{nm}$, and $\gamma = 89°$) reveal a slight (sub-nanometer) deviation from the gyroid cubic symmetry in the out-of-plane [110] direction; the unit cell parameters, but not the morphology, can vary substantially as a function of SVA parameters (see below). Figure 1(c) shows a representative atomic force microscopy (AFM) image of an ISO film after annealing in the mixed vapors of tetrahydrofuran (THF) and methanol (80:20) and subsequent quenching. The film surface features a regular dot array corresponding to the (110) plane of a body-centered cubic lattice with a

lateral unit cell size $a = 34.5\,\text{nm}$ as determined by the fast Fourier transform (FFT) of the image, and thus is both qualitatively and quantitatively consistent with the indexed single gyroid morphology. The alternating gyroid morphology of the ISO terpolymer, consisting of two enantiomorphic single gyroid networks of PI ($f_{\text{PI}} = 0.31$) and PEO ($f_{\text{PEO}} = 0.17$) is shown in Figure 1(d).

Solvent Vapor Annealing (SVA) Regimes

Different SVA morphological "regimes" were identified in the ISO films by observing changes in the scattering patterns as a function of swelling ratio φ, the ratio of the swollen to dried film thicknesses. Figure 2 shows the eight regimes identified during the swelling and deswelling of an ISO film in the mixed vapors of THF and methanol (80:20). As readily determined by homopolymer dissolution experiments, THF is a good solvent for PS, PI, and PEO; methanol is a good solvent only for PEO (better than THF) and a poor solvent for PS and PI (see below). A THF-rich mixture of the two solvent vapors, as used here, is therefore anticipated to be a good solvent for all ISO blocks (see Methods). Figure 2 shows the GISAXS scattering patterns (Figure 2(a)), swelling ratios (Figure 2(b)), line integral surfaces (Figure 2(c)), and in-plane scattering peak metrics (Figures 2(d) and 2(e)) corresponding to the eight SVA regimes. The variation of the line integral surfaces with swelling ratio corresponds to in-plane variations of the $[1\bar{1}0]$ peaks at their out-of-plane wave vector $q_z^{[1\bar{1}0]}$ (cf. Figure 1). The scattering peak metrics show the variation of the position of the $[1\bar{1}0]$ peaks $q_y^{[1\bar{1}0]} \approx \pm 0.026\,\text{Å}^{-1}$ (Figure 2(d)) and width $\Delta q_y^{[1\bar{1}0]}$ (Figure 2(e)) during swelling and deswelling in the ordered regimes, calculated from the GISAXS line integrals. The eight SVA regimes and their corresponding onset swelling ratios* are identified as follows:

i. As-Spun: After spin-coating and before application of solvent vapor ($\varphi = 1.00$), the GISAXS scattering pattern exhibits significant intensity along the entirety of the "dif-

*The onset swelling ratios corresponding to regimes *ii* – *iv* depend on the swelling rate, as chain motion and thus ISO self-assembly are kinetically limited at low solvent concentrations due to slow chain diffusion close to the plasticization regime.

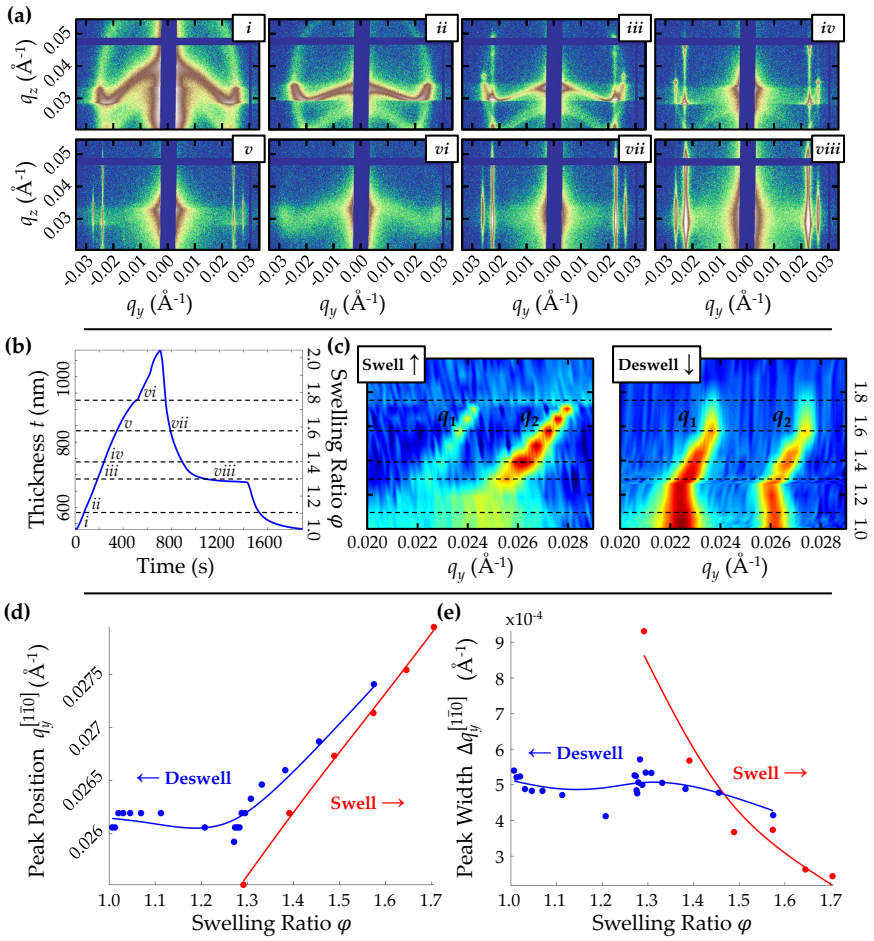

Figure 2: **Solvent vapor annealing (SVA) regimes during swelling and deswelling of an ISO film.** Eight SVA "regimes" were identified during the swelling and deswelling of an ISO film in the mixed vapors of THF and methanol (80:20). (a) Representative GISAXS patterns for the eight SVA regimes, acquired at a fixed angle of incidence ($\alpha_i = 0.18°$). The regimes and corresponding onset swelling ratios (φ) are labeled as: *i. As-Spun* (1.00); *ii. Plasticization* (1.10); *iii. Ordering* (1.29); *iv. Order* (1.39); *v. Approaching Disorder* (1.57); *vi. Disorder* (1.74); *vii. Re-Ordering* (1.57); and *viii. Vitrification* (1.29). The logarithmic color scales were normalized to the maximum and minimum intensities of each pattern. (b) Film thickness and swelling ratio as a function of time. (c) Swelling and deswelling line integral surfaces: the line integral of the GISAXS pattern at the out-of-plane wave vector $q_z^{[1\bar{1}0]}$ is plotted as a function of swelling ratio (cf. Figure 1). The logarithmic color scales were normalized to the maximum and minimum intensities of each complete set of line integrals. (d) Peak position $q_2 = q_y^{[1\bar{1}0]}$ and (e) width $\Delta q_2 = \Delta q_y^{[1\bar{1}0]}$ (full width at half maximum) of the peak at $q_y \approx 0.026\,\text{Å}^{-1}$ (q_2) during swelling (red) and deswelling (blue). The peak metrics were calculated from the GISAXS line integrals. The solid lines are guides to the eye.

fuse Debye-Scherrer ring" (DDSR) spanning the $q_y q_z$ plane at $q_y \approx \pm 0.025\,\text{Å}^{-1}$ and $q_z \approx 0.04\,\text{Å}^{-1}$.[34] This high intensity DDSR includes contributions from both the "reflected" and "transmitted" beams and appears as a broad single peak in the line integral surface (cf. Figure 1).[39] The significant presence of a DSSR is indicative of a poorly ordered isotropic microphase-separated morphology.

ii. Plasticization: As the solvent concentration in the film increases ($\varphi \approx 1.10$), the GISAXS pattern begins to change. The locus of the high intensity DDSR shifts to lower q_z values. This indicates plasticization of the polymer (i.e. a lowering of the glass transition temperature T_g^{PS} of the PS matrix below ambient temperature) and relaxation of the as-spun morphology.

iii. Ordering: As the solvent concentration in the film is increased ($\varphi \approx 1.29$), the intensity of the DDSR reduces and distinct Bragg reflections begin to appear. Similarly, the line integral surface begins to exhibit two laterally separate signals, labeled q_1 and q_2. The q_1 signal is associated with the reflected and transmitted [101] and transmitted [211] peaks of the alternating gyroid morphology; the q_2 signal is associated with the reflected and transmitted $\left[1\bar{1}0\right]$ peaks, i.e. $q_2 = q_y^{[1\bar{1}0]}$ (cf. Figure 1). The appearance of distinct Bragg reflections indicates the onset of ordering in the polymer film.

iv. Order: With a further increase in solvent concentration ($\varphi \approx 1.39$), the DDSR disappears and distinct, pronounced Bragg reflections appear at $q_y \approx \pm 0.023\,\text{Å}^{-1}$ and $q_y \approx \pm 0.026\,\text{Å}^{-1}$. The peak metrics corresponding to $q_2 = q_y^{[1\bar{1}0]}$ in Figures 2(d) and 2(e) exhibit an increase in $q_y^{[1\bar{1}0]}$ and reduction in $\Delta q_y^{[1\bar{1}0]}$, respectively, with increasing solvent concentration. The disappearance of the DDSR and the increased intensity of the Bragg reflections indicates that the copolymer has assembled into a well-ordered morphology that is consistent with the alternating gyroid (cf. Figure 1). The increase in $q_y^{[1\bar{1}0]}$ with φ and the reduction in $\Delta q_y^{[1\bar{1}0]}$ indicate a slight decrease in the gyroid lateral unit cell size with increasing long-range order.

v. Approaching Disorder: Upon further increase in solvent concentration ($\varphi \approx 1.57$), the distinct signal variation in q_z for the Bragg reflections at $q_y \approx \pm 0.023\,\text{Å}^{-1}$ and $q_y \approx \pm 0.026\,\text{Å}^{-1}$ smear-out into so-called "diffuse Bragg rods". Interestingly, the quality of the in-plane order continues to increase, witnessed by a decrease in $\Delta q_y^{[1\bar{1}0]}$ in Figure 2(e).

The narrowing of the in-plane reflection peaks indicates, on the one hand, the continued presence and improved ordering of the gyroid morphology in at least part of the film, evident when probed over large in-plane areas. The loss of distinct out-of-plane peaks into Bragg rods indicates, on the other hand, a loss of the periodic morphology spanning across the entire thickness of the film, which may arise from interfacial disorder, as discussed below.

vi. Disorder: Approaching the the highest explored solvent concentration of $\varphi \approx 1.74$, the diffuse Bragg rods disappear and only a very faint DDSR is visible in the GISAXS patterns, reducing the line integral surface to zero. The disappearance of the Bragg rods indicates the absence of a microphase-separated morphology, i.e. disorder.

vii. Re-Ordering: As the solvent concentration is decreased ($\varphi \approx 1.57$), the diffuse Bragg rods at $q_y \approx \pm 0.023\,\text{Å}^{-1}$ and $q_y \approx \pm 0.026\,\text{Å}^{-1}$ begin to reappear in the GISAXS pattern and the deswelling line integral surface. The peak $q_2 = q_y^{[1\bar{1}0]}$ reduces in its q_y value on a trajectory similar to that during swelling and broadens slightly. The reappearance of the Bragg rods indicate that the terpolymer has begun to self-assemble towards its equilibrium microphase-separated morphology. The peak metrics indicate that the lateral unit cell is slightly increased and the degree of order is lower compared to regime *vi*.

viii. Vitrification: As the solvent concentration is further decreased ($\varphi \approx 1.29$), the diffuse Bragg rods increase in intensity and the $q_2 = q_y^{[1\bar{1}0]}$ peak remains at a stationary q_y value and peak width. The GISAXS pattern, deswelling line integral surface, and peak

metrics do not change any further as remaining solvent is removed. The stability of the peak metrics indicates the vitrification of at least one of the copolymer domains (almost certainly the PS), immobilizing the entire terpolymer morphology. For high T_g polymers, vitrification typically sets in at substantial swelling ratios.

The behavior of ISO during annealing with different THF and methanol solvent vapor mixtures is explored below.

Effect of the Maximum Swelling Ratio and Solvent Removal Rate

Having identified the various regimes observed during SVA of ISO films, the SVA parameter space was explored with the aim of maintaining the highly ordered state of the swollen microphase-separated morphology (i.e. regime *iv* in Figure 1(a)) in the dried film. To this end, the coupled effect of quenching the film from either the disordered regime (close to disorder) or the ordered regime (determined by the maximum swelling ratio), and the rate of solvent removal, were investigated. Figure 3 shows four SVA protocols together with GISAXS scattering patterns in the swollen and dried states. The mixed solvent vapors of THF and methanol (80:20) were used.

Table 2: Peak metrics (q_y peak positions and full widths at half maximum) corresponding to the dried film morphologies of ISO films annealed in the mixed vapors of THF and methanol (80:20), quenched from the disordered and microphase-separated swollen regimes at differing quenching rates.

Quench from $\varphi_{max} \approx$	2.0	1.6	1.3	1.3
Quench rate (nm/s)	4.59	1.07	1.69	0.21
$q_y^{[1\bar{1}0]}$ (Å^{-1})	0.0261	0.0265	0.0255	0.0257
$\Delta q_y^{[1\bar{1}0]}$ ($\times 10^{-4}$ Å^{-1})	5.40	6.30	7.72	7.40

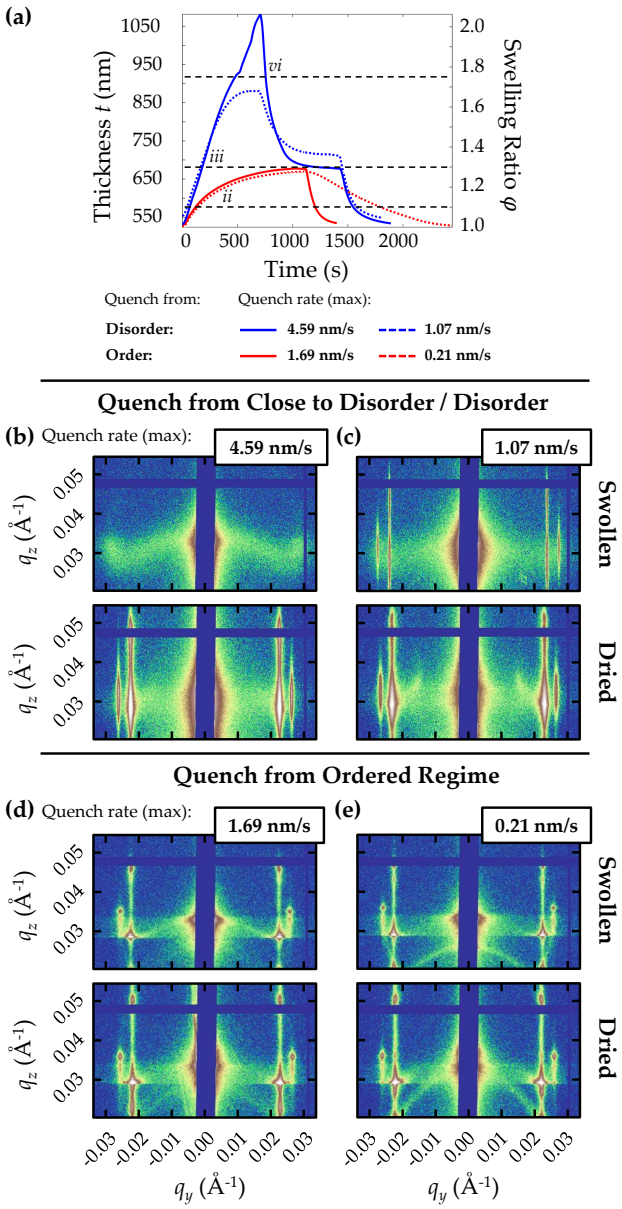

Figure 3: **Effect of maximum swelling ratio and solvent removal rate on the dried film morphology.** Film thickness profiles and GISAXS patterns of swollen and dried films subjected to different solvent removal (quench) rates after swelling to different maximal swelling ratios $\varphi_{\max}$. All films were annealed in mixed vapors of THF and methanol (80:20). (a) Film thickness (swelling ratio) profiles of four films subjected to SVA. Two films were quenched from $\varphi_{\max} > 1.3$ (blue lines) with maximal quench rates of 4.59 nm/s and 1.07 nm/s, respectively. Two further films were quenched from $\varphi_{\max} \approx 1.3$ (red lines) with maximal solvent removal rates of 1.69 nm/s and 0.21 nm/s, respectively. (b) – (e) GISAXS patterns ($\alpha_i = 0.18°$) of the swollen (top row) and dried (bottom row) films for the four cases. The logarithmic color scales were normalized to the maximum and minimum intensities of each pattern.

Maximum swelling ratio. Three different maximum swelling ratios were chosen. The two films marked in blue in Figure 3(a) were swollen to $\varphi_{\max} \approx 1.6$ and 2.0, closely below and well above the disorder transition, respectively, as confirmed by the GISAXS patterns of the maximally swollen films in Figures 3(b) and 3(c). Only the film swollen to $\varphi_{\max} \approx 2.0$ lack any GISAXS scattering peaks, while the film swollen to $\varphi_{\max} \approx 1.6$ is found to result in distinct peaks in q_y but broad peaks in the q_z direction, as described above (regime *v*). Two further films, marked by red lines in Figure 3(a), were brought into the ordered regime[†] (i.e. regime *iv*) by slowly swelling to $\varphi_{\max} \approx 1.3$, as confirmed by the appearance of distinct, pronounced peaks in both q_y and q_z in the GISAXS patterns of the swollen state in Figures 3(d) and 3(e).

The comparison of Figures 3(b) – 3(e) shows that it is beneficial to quench from the well-ordered swollen state at $\varphi_{\max} \approx 1.3$ compared to a higher swelling ratio. While all quenched films exhibit in-plane order with comparable peak-widths, only the samples quenched from $\varphi_{\max} \approx 1.3$ exhibit the full range of q_y and q_z peaks that can be confidently assigned to the alternating gyroid morphology based on indexing the corresponding GISAXS patterns (not shown; cf. Figure 1).

The line integral surfaces in Figure S1 and their analysis in Figure S2 give further insight into quenching from differing $\varphi_{\max}$ values. Focusing on the deswelling of the four samples, clear differences between the $\varphi_{\max} > 1.3$ and $\varphi_{\max} \approx 1.3$ samples emerge. For the former, an evolution in $q_y^{[1\bar{1}0]}$ peak position and $\Delta q_y^{[1\bar{1}0]}$ width is observed when quenching from $\varphi_{\max}$ to $\varphi \approx 1.3$. In all samples the $q_y^{[1\bar{1}0]}$ peak position does not change upon quenching below $\varphi \approx 1.3$ and the peak width increases only slightly. This indicates that two separate relaxation processes are active within the drying films and that the order that is present in the film for $\varphi \approx 1.3$ determines the order in the dry film. It appears that in the films quenched from $\varphi_{\max} > 1.3$, the sample did not have sufficient time to reorder, and their poor

[†]Note that the swelling rate applied here is much smaller than in Figure 2. At such a small swelling rate the film is effectively being annealed, which allows generating a well-ordered structure even slightly below the onset swelling ratio of the ordered regime in Figure 2.

q_z order (Bragg rods rather than distinct reflection peaks) is preserved in the dry films.

A quantitative analysis of the peak metrics (Table 2, Figure S2) shows that films quenched from $\varphi_{\max} > 1.3$ lie at slightly higher q_y values and they are somewhat narrower, compared to those quenched from $\varphi_{\max} \approx 1.3$.

Solvent removal rate. Since slow quenching from high φ values is very time consuming, only two representative samples were explored. The similarity of the GISAXS patterns of the dried films in Figures 3(b) and 3(c) indicates that the solvent removal rate does not significantly affect the structure in the films that were quenched from $\varphi_{\max} > 1.3$. The two samples quenched from $\varphi_{\max} \approx 1.3$, on the other hand, maintain the distinct peak structure along the q_z direction (Figures 3(d) and 3(e)). This indicates that $\varphi_{\max}$ is the dominant parameter, with the quench rate having only a minor influence on the organization of the microphase-separated morphology. This is borne out by the scattering peak parameters (Table 2 and Figures S2), which are quantitatively similar for the samples quenched from $\varphi_{\max} \approx 1.3$ and $\varphi_{\max} > 1.3$, respectively.

Effect of Drying

The characteristics of the 3D lattice of the alternating gyroid in solvent-annealed ISO films were determined by indexing GISAXS patterns (see Methods, cf. Figure 1). Figure 4 shows indexed patterns of an ISO film annealed in a solvent vapor mixture of THF and methanol (50:50). The 2D peak patterns in the swollen (Figure 4(a)) and dried state (Figure 4(b)) look qualitatively similar and both were successfully indexed with the space group $I4_132$ (Q^{214}) of the alternating gyroid with the [110] direction oriented out-of-plane. However, only the swollen state structure shows a nearly-ideal cubic unit cell ($a = b = 36.2\,\text{nm}$, $c = 35.5\,\text{nm}$, and $\gamma = 89°$), whereas in the dried state the cubic lattice is significantly distorted. The unit cell of the dried film structure, $a = b = 32.6\,\text{nm}$, $c = 36.0\,\text{nm}$, and $\gamma = 101°$, is evidently deviating from a cubic lattice. Note that drying the films results in a decrease in a and b

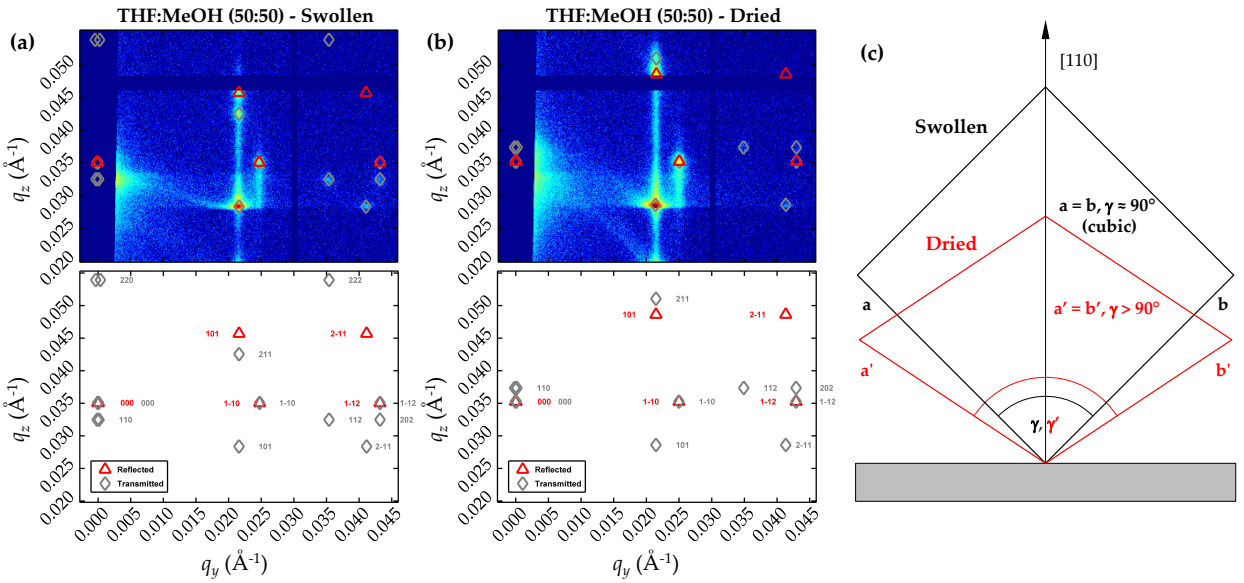

Figure 4: **Effect of drying on the cubic lattice of solvent-annealed ISO films.** Indexed 2D GISAXS patterns (top row) and corresponding reflections labeled with Miller indices (bottom row) of (a) swollen and (b) dried ISO films annealed in mixtures of THF and methanol (50:50). The indexed reflections correspond to peaks of the $I4_132$ space group with the [110] direction oriented perpendicular to the substrate using the following unit cell parameters: (a) $a = b = 36.2\,\text{nm}$, $c = 35.5\,\text{nm}$, and $\gamma = 89°$ for the swollen film, and (b) $a = b = 32.6\,\text{nm}$, $c = 36.0\,\text{nm}$, and $\gamma = 101°$ for the dried film. (c) Schematic of the observed lattice changes in the [110] (out-of-plane) direction upon quenching.

while c is found to increase. The changes of the lattice parameters upon drying correspond to a shrinkage of the unit cell along the [110] direction as schematically shown in Figure 4(c). Note that similar effects were observed for ISO films annealed in varying compositions of mixed THF and methanol vapors (e.g. the effects of solvent vapor composition; see below).

Effect of Solvent Vapor Composition

In addition to the maximum swelling ratio and quench rate, the selectivity of the microphase-separated domains to the solvent vapor (or mixture of solvent vapors) is a further crucial SVA parameter which may affect the microphase-separated morphology and its long-range order. The SVA experiments presented above mainly used mixed solvent vapors of THF and methanol (80:20). The three PS, PI, and PEO microphase-separated domains are likely to exhibit different selectivities to the more polar methanol or the more apolar THF, which

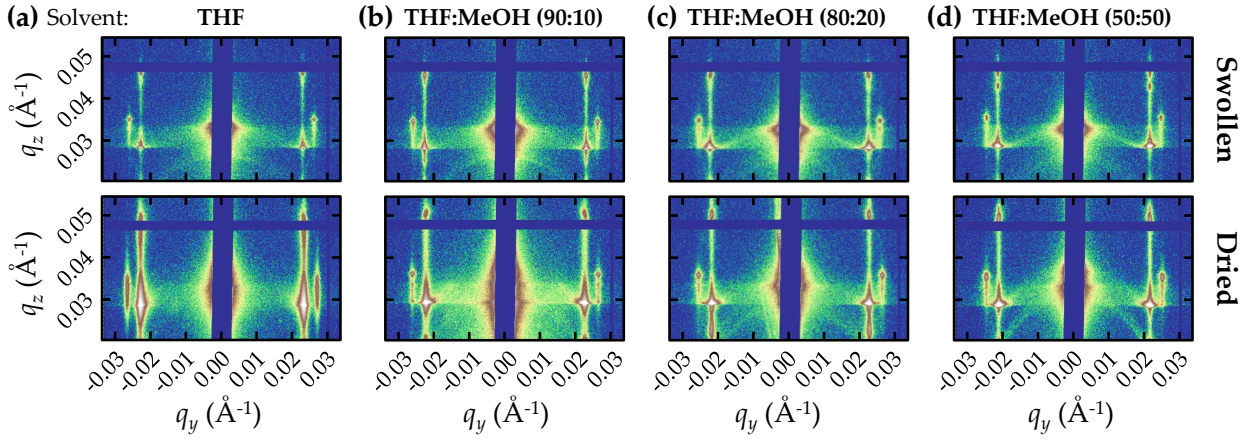

Figure 5: **Effect of solvent vapor composition on the morphology of swollen and dried ISO thin films.** GISAXS patterns ($\alpha_i = 0.18°$) investigating the effect of solvent vapor composition on the swollen and dried microphase-separated morphologies of ISO films quenched from (a) $\varphi_{max} \approx 1.6$ and (b)–(d) $\varphi_{max} < 1.4$ (cf. Figure 2). The mixed solvent vapors used to anneal the films were (a) THF, (b) THF and methanol (THF:MeOH) (90:10), (c) THF:MeOH (80:20), and (d) THF:MeOH (50:50). The logarithmic color scales were normalized to the maximum and minimum intensities of each pattern.

Table 3: Maximum swelling ratio (φ_{max}), approximate swelling ratio corrseponding to the "ordering" regime (φ_{iii}), maximum swelling rate, and maximum quench rate for films annealed in THF and three THF and methanol mixtures (THF:MeOH).

Solvent	φ_{max}	φ_{iii}	**Swell rate (nm/s)**	**Quench rate (nm/s)**
THF	1.54	1.20	1.11	0.99
THF:MeOH (90:10)	1.37	1.25	0.75	0.45
THF:MeOH (80:20)	1.27	1.24	0.63	0.69
THF:MeOH (50:50)	1.23	1.22	0.77	1.32

may lead to morphological transitions in the ISO terpolymer film. The effects of annealing in solvent vapors of different compositions on the swollen and dried microphase-separated morphologies were therefore investigated in Figures 5, 6 and 7.

Figure 5 shows the GISAXS patterns of swollen (top row) and dried (bottom row) ISO films annealed in varying compositions of mixed THF and methanol vapors. The corresponding swelling and deswelling line integral surfaces are shown in Figure S4. While all four swollen films have very similar GISAXS patterns with distinct peaks both in q_y and q_z (Figure 5), this pattern is retained upon drying only in the films dried from swollen, but not in the film swollen in pure THF, where the peaks in q_z direction broadened significantly in the dry film. This deterioration of out-of-plane order probably arises from a swelling ratio much closer to the disorder transition ($\varphi_{\max} \approx 1.54$, regime *v*), compared to the other samples (maximum swelling ratio $\varphi_{\max} \approx 1.23 - 1.37$, Table 3).

The lowest swelling ratio (φ_{iii}) at which the peak at $q_y \approx 0.026\,\text{Å}^{-1}$ ($q_2 = q_y^{[1\bar{1}0]}$; cf. Figure 2(c)) associated with the "ordering" regime (regime *iii*) appears for each of the samples in Figure 5 is given in Table 3. When comparing samples that were swollen with $\varphi_{\max}$ sufficiently close to φ_{iii}, it is clear that the effect of the solvent mixing ratio is relatively small.

A careful analysis of Figure 6 however, reveals the detailed effects of the solvent mixing ratio on the ISO microphase-separated morphology. Considering Figure 6(b), it is clear that the $q_2 = q_y^{[1\bar{1}0]}$ peak position decreases with increasing methanol content. But since the disorder transition (and hence the boundaries of the regimes described above) also vary with methanol content, it is difficult to disentangle thermodynamic and kinetic effects. It is therefore instructive to also consider the peak positions during swelling (Figure 6(a)). With increasing methanol content, the peak position $q_y^{[1\bar{1}0]}$ becomes increasingly sensitive to the swelling ratio (i.e. the slope $\mathrm{d}q_y^{[1\bar{1}0]}/\mathrm{d}\varphi$ increases with increasing methanol content).

During swelling, the associated peak widths at $q_y \approx 0.026\,\text{Å}^{-1}$ ($\Delta q_y^{[1\bar{1}0]} = \Delta q_2$) follow a similar trend and narrow increasingly rapidly with increasing methanol content (Figure 6(c)),

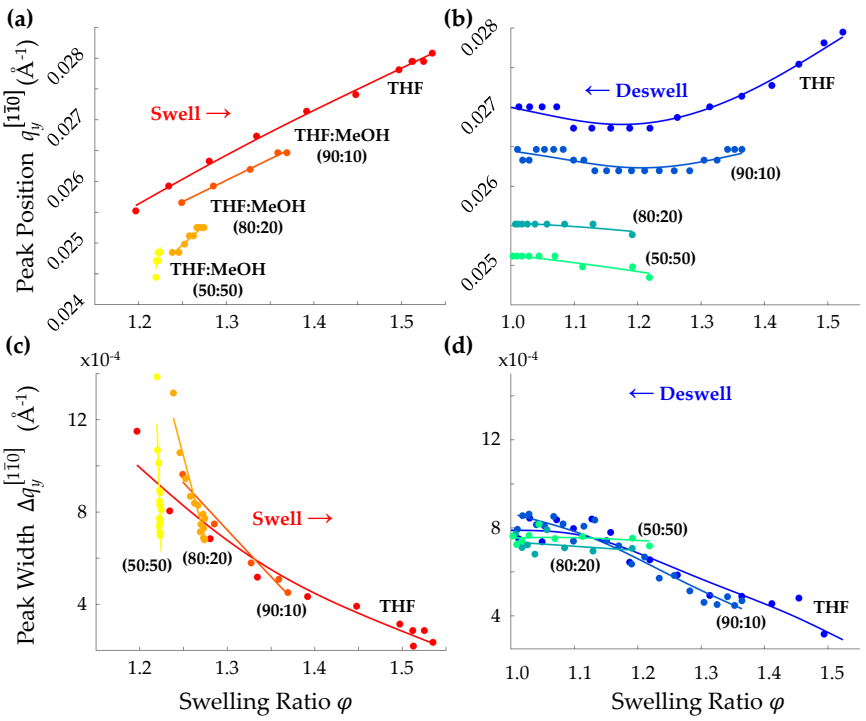

Figure 6: **Effect of solvent vapor composition on the GISAXS peak positions and widths of ISO thin films during swelling and deswelling.** Positions of the $q_y^{[1\bar{1}0]} \approx 0.026\,\text{Å}^{-1}$ peak (q_2) and their widths $\Delta q_y^{[1\bar{1}0]}$ during (a) and (c) swelling and (b) and (d) deswelling of ISO thin films annealed in THF and three THF/methanol mixtures. The peak metrics were calculated from the corresponding GISAXS line integrals.

with the lowest absolute values for pure THF. This trend is much less evident in the deswelling curves of Figure 6(d). Note that unlike the maximum swelling ratio, the maximum swell rate and quench rate of each of the films do not vary monotonically with the proportion of THF in the mixture of solvent vapors (Table 3).

The characteristics of the 3D lattice of the alternating gyroid in ISO films annealed in varying compositions of mixed THF and methanol vapors were determined by indexing of the GISAXS images in Figure 5 (cf. Figure 4). Figure 7 compares the drying-induced changes of the unit cell parameters of ISO films annealed in THF and three THF and methanol mixtures. In the swollen state, the unit cells are approximately cubic with an increasing deviation from an ideal cubic structure with increasing maximum swelling ratio (increasing methanol content) (Figures 7(a) and 7(b)). The smallest observed deviation from an ideal cubic unit cell (about 2%) is seen for a symmetric composition of THF and

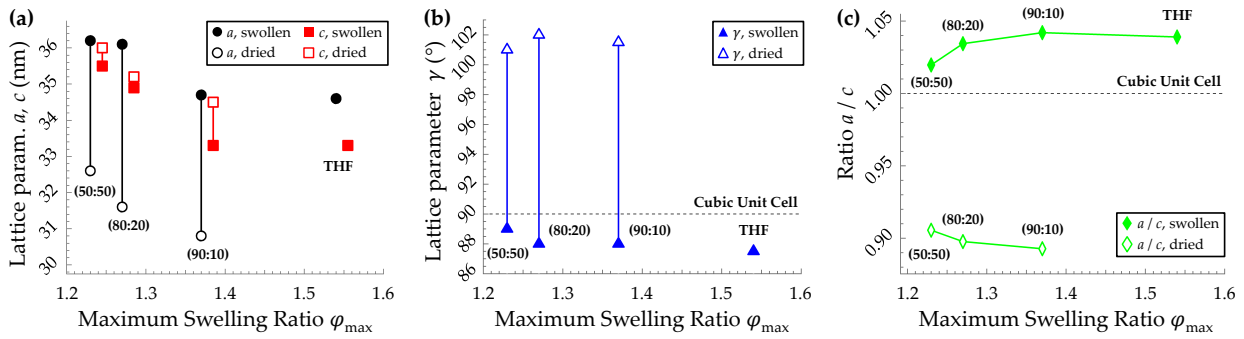

Figure 7: **Effect of solvent vapor composition on lattice parameters of swollen and dried ISO thin films.** Lattice parameters (a) a and c, (b)γ, and (c) the ratio a/c of the ISO films annealed in THF and three THF and methanol mixtures in the swollen and dried films as a function of the maximum swelling ratio $\varphi_{\max}$. The lattice parameters were determined by indexing the 2D GISAXS images shown in Figure 5 and as demonstrated in Figure 4.

methanol (Figure 7(c)). In the dried films the cubic unit cells are, however, significantly distorted for all THF and methanol mixing ratios (Figures 7(a) and 7(b)), again with the smallest effect ($a/c \approx 0.91$, Figure 7(c)) for the smallest maximum swelling ratio (the highest methanol content, THF:MeOH (50:50)). The distortion of the cubic lattice upon drying is schematically shown in Figure 4(c). Note that such an out-of-plane distortion of the alternating gyroid is also observed in thermally annealed films, but to a much smaller extent ($a/c \approx 0.96$, $\gamma = 94°$ after annealing at 160°C and subsequent quenching, Figure S3).

Discussion

As in any annealing experiment, structure evolution by self-assembly is determined by the interplay of thermodynamic parameters (the path through phase space) and the kinetics of parameter evolution. In the case of SVA, this is further complicated by the changing overall volume: the solvent from the vapor phase is itself part of the thermodynamic system and influences the kinetics determined by the experimental protocol. The present study aims to improve our understanding of this complex system in the context of network-forming triblock terpolymers.

The as-spun film initially exhibits a kinetically-trapped isotropic microphase-separated morphology with only short-range order.[25] Upon plasticization due to solvent uptake, the film self-assembles towards its (solvated) equilibrium microphase-separated morphology. The ISO employed in this study, with its relative block lengths (see Methods) and the relative strength of the three Flory-Huggins interaction parameters ($\chi_{IO} > \chi_{IS} \approx \chi_{SO}$), forms an alternating gyroid in both thermally annealed bulk samples[22] and the solvent-annealed films studied here (Figures 1(a) – 1(c)). In the ISO alternating gyroid, the PI and PEO blocks form the two interpenetrating single gyroid networks separated by the continuous matrix of the PS block (Figure 1(d)). Since the PS matrix is glassy at room temperature—while PI and PEO both are well above their respective T_gs—ISO plasticization is governed by the solvent uptake of PS. As the solvent concentration in the film increases, the degree of order of the alternating gyroid morphology improves, both in- and out-of-plane. Using the Scherrer equation,[40] i.e. $\Delta d = K \times 2\pi/\Delta q_y^{[1\bar{1}0]}$, where $K \approx 0.93$, the lateral grain size is $\Delta d \approx 0.63\,\mu m$ upon ordering, improving to $\Delta d \approx 2.40\,\mu m$ before disordering.[‡] At the same time, the gyroid lateral unit cell size (i.e. $d = \sqrt{2} \times 2\pi/q_y^{[1\bar{1}0]}$) decreases as the swelling ratio is increased, from 34.8 nm upon ordering to a minimum of 31.8 nm just below the disorder transition. This decrease in lateral unit cell size points to a solvent-mediated reduction in the three Flory-Huggins interaction parameters at high swelling ratios, and therefore a reduction in the net segregation strength of the terpolymer.

Note that the simultaneous swelling of the film with a reduction in unit cell size implies a substantial reorganization of the gyroid morphology, since the number of gyroid lattice unit cells has to significantly increase to reconcile a simultaneous increase in film thickness with a (small) reduction in the lattice constants. This is similar to the swelling of cylindrical[8] and lamellar[33?] morphologies.

As the solvent concentration is further increased, order in the alternating gyroid morphology begins to deteriorate in the out-of-plane direction while it continues to improve in

[‡]Note that this estimate does not take the instrument-related peak broadening into account. The given values are therefore lower bound estimates.

the plane. Since there is very little change in the $q_y^{[1\bar{1}0]}$ signal, part of the film remains an ordered gyroid, while another part (most likely layers at one or both film surfaces) loses the gyroid morphology, transforming to a disordered morphology, an ordered morphology that is not periodic in 3D (e.g. lamellae), or into a mixed state. Morphological surface reorganization upon approaching the disorder transition is not surprising, since with the three Flory-Huggins interaction parameters approaching zero, surface interactions become increasingly important.

Upon deswelling from disorder, the alternating gyroid morphology reappears and the lateral unit cell size once again increases until the onset of vitrification at a unit cell size of 34.1 nm. Although significantly improved compared to the as-spun film, the dry film has a lower degree of order compared to the swollen film, both in- and out-of-plane (cf. Figure 2(e)), with a lateral grain size in the dried film of $\approx 1.08\,\mu$m. This much lower degree of order arises again from the substantial morphological reorganization imposed on the terpolymer morphology. The drying of the film causes a simultaneous volume reduction and increase in the three Flory-Huggins parameters requiring a significant reduction in number of gyroid unit cells in the out-of-plane direction. However, the increase in film viscosity with decreasing solvent content slows down the reorganization of the gyroid lattice and suppresses it entirely once the PS matrix is vitrified. This slowing-down and freezing-in of the continuously reorganizing microphase-separated morphology results in the observed decreased order within the vitrified film.

The kinetics of the structural reorganization is seen in the GISAXS line integral plots of Figure 2(c). During swelling, both the peak position $q_y^{[1\bar{1}0]}$ and width $\Delta q_y^{[1\bar{1}0]}$ vary monotonically (approximately linearly) with the swelling ratio. The variation of $q_y^{[1\bar{1}0]}$ and $\Delta q_y^{[1\bar{1}0]}$ during deswelling resemble that of the swelling plot (albeit with a different slope) for swelling ratios above $\varphi \approx 1.3$. However, both quantities vary very little upon further solvent removal for $\varphi < 1.3$. This indicates the existence of two different quenching regimes, where for $\varphi > 1.3$ the morphology is sufficiently mobile to allow the continuous reorganization of

the microphase-separated morphology upon change in swelling ratio, while for $\varphi < 1.3$ the microphase-separated morphology is essentially immobile. As a consequence the gyroid morphology freezes in before the film is completely dried. This discrepancy between the kinetics of structural reorganization and drying creates a problem. As the film thickness continues to decrease during the drying process, the already-vitrified gyroid morphology ($\varphi < 1.3$) begins to distort in the out-of-plane direction as shown in Figure 4. This results in a significant out-of-plane distortion ($\approx 10\%$) of the cubic lattice of the alternating gyroid in dried films.

In this context it is instructive to revisit two different quenching conditions. A rapid quench from a swollen film with $\varphi_{\max} \gg 1.3$ preserves the high degree of in-plane order and the smaller lateral unit-cell size of the swollen gyroid (i.e. kinetically arresting morphological reorganization during deswelling). Unfortunately, the small degree of out-of-plane order is also preserved. On the other hand, annealing the sample at $\varphi \approx 1.3$ allows the system to attain a reasonable in- and out-of-plane order, which changes only little upon quenching. A variation of the quench rate does not seem to play an important role, neither for quenching from $\varphi > 1.3$ nor from $\varphi \approx 1.3$. A very slow quench from $\varphi \approx 1.3$, however, improves the order somewhat.

Clearly, these two cases illustrate a compromise when designing SVA protocols for gyroid terpolymer films with the aim of achieving long-range order both in and out-of the plane of the film. High swelling ratios are required for optimal in-plane order but this comes at the expense of potentially poorer out-of-plane order, i.e. the film does not have the same microphase-separated morphology across its entire thickness. Equilibrating the films at a "sweet-spot" swelling ratio (here $\varphi \approx 1.3$), on the other hand, enables good out-of-plane order but at the expense of the in-plane order of the microphase-separated morphology.

Varying the ratio of the THF and methanol in the solvent vapor mixture adds a further degree of freedom to the experimental parameter space. Given the strong selectivity of methanol for PEO, the insensitivity of the results of Figure 5 is surprising. Selective swelling of one of the domains often leads to morphological transitions, as found for example in diblock

copolymers.[14] The lack of such a transition in the ISO triblock terpolymer system arises from the relatively large composition window in the ISO phase diagram for which the alternating gyroid morphology is reported. This is in sharp contrast to the narrow double gyroid region in the phase diagram of diblock copolymers.[18,41] Clearly, the molecular composition of the ISO used in this study places its equilbirium morphology firmly within alternating gyroid phase space, as indeed intended (see Methods).[42]

Since the swelling of the ISO film is governed by the PS matrix phase, the main effect of the THF and methanol ratio lies in the maximum swelling ratio attainable for a given flow rate of solvent vapor and temperatures of sample and solvent, which decreases markedly with increasing methanol content. This has a strong effect on the swollen ISO unit cell size. Since the unit cell size is typically frozen-in during the quench (see above), the main effect of the solvent composition lies in the final gyroid lattice constant. The in-plane order, as measured through the peak width $\Delta q_y^{[1\bar{1}0]}$, is affected very little by the THF and methanol ratio.

Conclusion

This study investigates in detail the phase behavior of a gyroid-forming ISO triblock terpolymer upon swelling and quenching from a THF and methanol solvent vapor atmosphere. The system can be described in eight morphological swelling and deswelling regimes that straddle the dry film and a mixed ISO "solution" film. Attempts to equilibrate the ISO morphology in the swollen state and preserve its order in the quenched film are fundamentally limited by the thermodynamic requirement of the polymer to readjust its microphase-separated morphology with the swelling ratio. Within the 3D network morphology, this requires diffusive transport of the chains, which becomes increasingly difficult (from both a thermodynamic and kinetic point of view) as the sample is quenched.

Two scenarios were found, which present the experimenter with a conundrum. Quenching

from a highly swollen state (either ordered or disordered) results in a high degree of lateral (in-plane) order, but the film is not ordered across its entire thickness. Quenching from a less swollen microphase-separated state, exhibiting order both in- and out-of-plane across the entire film, allows to retain the microphase-separated morphology with 3D order in the dried film, but at expense of a high degree of in-plane order. The dominant control parameter for this is the maximum swelling ratio, with the swelling and quench rates modifying the microphase-separated morphology only very little within the range of parameters explored. The experiments further reveal a significant distortion of the cubic unit cell in dried films in the out-of-plane direction (i.e. the "direction of drying"), a fundamental obstacle toward achieving true 3D order in solvent-annealed gyroid films.

These results contribute towards the rational design of SVA protocols for the successful fabrication of large grains of the alternating gyroid morphology in triblock terpolymers, for example for optical metamaterial applications.[5,6,43,44] The robustness of the alternating gyroid morphology with respect to all varied SVA parameters is of great benefit as it ensures that the gyroid morphology is remarkably robust with respect to the SVA protocol. While the gyroid grain sizes achieved in this study were still limited to micrometer range, the discovered protocol suggest possible improvements. For example, oscillating the sample between different swelling ranges, or designing a staged deswelling protocol, may provide ways to improve lateral order and limit out-of-plane distortion, without sacrificing the morphology spanning the film.

Acknowledgement

This research was supported through the Swiss National Science Foundation through grant numbers 163220 (U.S.) and 168223 (B.D.W.), the National Center of Competence in Research Bio-Inspired Materials (U.S., B.D.W, I.G.), the Adolphe Merkle Foundation (B.D.W., U.S., I.G.), the Engineering and Physical Sciences Research Council through the Cambridge

NanoDTC EP/G037221/1, EP/L027151/1, and EP/G060649/1 (R.D., J.A.D., J.J.B.), and ERC LINASS 320503 (J.J.B.). This project has also received funding from the European Union's Horizon 2020 research and innovation programme under the Marie Sklodowska-Curie grant agreement No 706329/cOMPoSe (I.G.). U.W. thanks the National Science Foundation (DMR-1409105) for financial support. We further acknowledge the Paul Scherrer Institut, Villigen, Switzerland for provision of synchrotron radiation beamtime at beamline X12SA (cSAXS) of the SLS and would like to thank Ana Diaz for assistance during the GISAXS experiments.

References

(1) Schacher, F. H.; Rupar, P. A.; Manners, I. Functional Block Copolymers: Nanostructured Materials with Emerging Applications. *Angew. Chem. Int. Ed.* **2012**, *51*, 7897–7921.

(2) Ruiz, R.; Kang, H.; Detcheverry, F. A.; Dobisz, E.; Kercher, D. S.; Albrecht, T. R.; de Pablo, J. J.; Nealey, P. F. Density Multiplication and Improved Lithography by Directed Block Copolymer Self-Assembly. *Science* **2008**, *321*, 936–939.

(3) Lin, C.-H.; Polisetty, S.; O'Brien, L.; Baruth, A.; Hillmyer, M. A.; Leighton, C.; Gladfelter, W. L. Size-Tuned ZnO Nanocrucible Arrays for Magnetic Nanodot Synthesis via Atomic Layer Deposition-Assisted Block Polymer Lithography. *ACS Nano* **2015**, *9*, 1379–1387.

(4) Bates, C. M.; Maher, M. J.; Janes, D. W.; Ellison, C. J.; Wilson, C. G. Block Copolymer Lithography. *Macromolecules* **2014**, *47*, 2–12.

(5) Vignolini, S.; Yufa, N. A.; Cunha, P. S.; Guldin, S.; Rushkin, I.; Stefik, M.; Hur, K.; Wiesner, U.; Baumberg, J. J.; Steiner, U. A 3D optical metamaterial made by self-assembly. *Adv. Mater.* **2012**, *24*, OP23–OP27.

(6) Dolan, J. A.; Saba, M.; Dehmel, R.; Gunkel, I.; Gu, Y.; Wiesner, U.; Hess, O.; Wilkinson, T. D.; Baumberg, J. J.; Steiner, U.; Wilts, B. D. Gyroid Optical Metamaterials: Calculating the Effective Permittivity of Multidomain Samples. *ACS Photonics* **2016**, *3*, 1888–1896.

(7) Baruth, A.; Seo, M.; Lin, C. H.; Walster, K.; Shankar, A.; Hillmyer, M. A.; Leighton, C. Optimization of long-range order in solvent vapor annealed poly(styrene)-block-poly(lactide) thin films for nanolithography. *ACS Appl. Mater. Interfaces* **2014**, *6*, 13770–13781.

(8) Gu, X.; Gunkel, I.; Hexemer, A.; Gu, W.; Russell, T. P. An in situ grazing incidence X-ray scattering study of block copolymer thin films during solvent vapor annealing. *Adv. Mater.* **2014**, *26*, 273–281.

(9) Gu, X.; Gunkel, I.; Hexemer, A.; Russell, T. P. Controlling Domain Spacing and Grain Size in Cylindrical Block Copolymer Thin Films by Means of Thermal and Solvent Vapor Annealing. *Macromolecules* **2016**, *49*, 3373–3381.

(10) Dehmel, R.; Dolan, J. A.; Gu, Y.; Wiesner, U.; Wilkinson, T. D.; Baumberg, J. J.; Steiner, U.; Wilts, B. D.; Gunkel, I. Confined Crystallization Enabled Optical Mapping of Large Gyroid Block Copolymer Domains in Polymer and Metamaterial Films. **2017**,

(11) Sinturel, C.; Morris, M.; Hillmyer, M. A. Solvent Vapor Annealing of Block Polymer Thin Films. *Macromolecules* **2013**, *46*, 5399–5415.

(12) Posselt, D.; Zhang, J.; Smilgies, D.-M.; Berezkin, A.; Potemkin, I. I.; Papadakis, C. M. Restructuring in Block Copolymer Thin Films: In-Situ GISAXS Investigations During Solvent Vapor Annealing. *Prog. Polym. Sci.* **2016**, In Press.

(13) Paik, M. Y.; Bosworth, J. K.; Smilges, D.-M.; Schwartz, E. L.; Andre, X.; Ober, C. K. Reversible morphology control in block copolymer films via solvent vapor processing: An in situ GISAXS study. *Macromolecules* **2010**, *43*, 4253–4260.

(14) Chavis, M. A.; Smilgies, D. M.; Wiesner, U. B.; Ober, C. K. Widely tunable morphologies in block copolymer thin films through solvent vapor annealing using mixtures of selective solvents. *Adv. Funct. Mater.* **2015**, *25*, 3057–3065.

(15) Gunkel, I.; Gu, X.; Sun, Z.; Schaible, E.; Hexemer, A.; Russell, T. P. An in situ GISAXS study of selective solvent vapor annealing in thin block copolymer films: Symmetry breaking of in-plane sphere order upon deswelling. *J. Polym. Sci. B* **2016**, *54*, 331–338.

(16) She, M.-S.; Lo, T.-Y.; Ho, R.-M. Controlled Ordering of Block Copolymer Gyroid Thin Films by Solvent Annealing. *Macromolecules* **2014**, *47*, 175–182.

(17) Wu, Y.-H.; Lo, T.-Y.; She, M.-S.; Ho, R.-M. Morphological Evolution of Gyroid-Forming Block Copolymer Thin Films with Varying Solvent Evaporation Rate. *ACS Appl. Mater. Interfaces* **2015**, *7*, 16536–16547.

(18) Bates, F. S.; Fredrickson, G. H. Block CopolymersDesigner Soft Materials. *Phys. Today* **1999**, *52*, 32.

(19) Meuler, A. J.; Hillmyer, M. A.; Bates, F. S. Ordered Network Mesostructures in Block Polymer Materials. *Macromolecules* **2009**, *42*, 7221–7250.

(20) Bates, F. S.; Schulz, M. F.; Khandpur, A. K.; Forster, S.; Rosedale, J. H.; Almdal, K.; Mortensen, K. Fluctuations, conformational asymmetry and block copolymer phase behaviour. *Faraday Discuss.* **1994**, *98*, 7–18.

(21) Khandpur, A. K.; Foerster, S.; Bates, F. S.; Hamley, I. W.; Ryan, A. J.; Bras, W.; Almdal, K.; Mortensen, K. Polyisoprene-Polystyrene Diblock Copolymer Phase Diagram near the Order-Disorder Transition. *Macromolecules* **1995**, *28*, 8796–8806.

(22) Epps, T. H.; Cochran, E. W.; Hardy, C. M.; Bailey, T. S.; Waletzko, R. S.; Bates, F. S. Network phases in ABC triblock copolymers. *Macromolecules* **2004**, *37*, 7085–7088.

(23) Epps, T. H.; Cochran, E. W.; Bailey, T. S.; Waletzko, R. S.; Hardy, C. M.; Bates, F. S. Ordered Network Phases in Linear Poly (isoprene-b-styrene-b-ethylene oxide) Triblock Copolymers. *Macromolecules* **2004**, *37*, 8325–8341.

(24) Albalak, R. J.; Capel, M. S.; Thomas, E. L. Solvent swelling of roll-cast triblock copolymer films. *Polymer* **1998**, *39*, 1647–1656.

(25) Morphological Development in Solvent-Cast Polystyrene-Polybutadiene-Polystyrene (SBS) Triblock Copolymer Thin Films. *Macromolecules* **1998**, *31*, 2569–2577.

(26) Albert, J. N. L.; Young, W.-S.; Lewis, R. L.; Bogart, T. D.; Smith, J. R.; Epps, T. H. Systematic Study on the Effect of Solvent Removal Rate on the Morphology of Solvent Vapor Annealed ABA Triblock Copolymer Thin Films. *ACS Nano* **2012**, *6*, 459–466.

(27) Seppala, J. E.; Lewis, R. L.; Epps, T. H. Spatial and orientation control of cylindrical nanostructures in ABA triblock copolymer thin films by raster solvent vapor annealing. *ACS Nano* **2012**, *6*, 9855–9862.

(28) Elbs, H.; Drummer, C.; Abetz, V.; Krausch, G. Thin Film Morphologies of ABC Triblock Copolymers Prepared from Solution. *Macromolecules* **2002**, *35*, 5570–5577.

(29) Fukunaga, K.; Elbs, H.; Magerle, R.; Krausch, G. Large-scale alignment of ABC block copolymer microdomains via solvent vapor treatment. *Macromolecules* **2000**, *33*, 947–953.

(30) Fukunaga, K.; Hashimoto, T.; Elba, H.; Krausch, G. Self-assembly of a lamellar ABC triblock terpolymer thin film. Effect of substrates. *Macromolecules* **2003**, *36*, 2852–2861.

(31) Shelton, C. K.; Epps, T. H. Block copolymer thin films: Characterizing nanostructure evolution with in situ X-ray and neutron scattering. *Polymer* **2016**, *105*, 545–561.

(32) Bai, W.; Yager, K. G.; Ross, C. A. In Situ Characterization of the Self-Assembly of a Polystyrene-Polydimethylsiloxane Block Copolymer during Solvent Vapor Annealing. *Macromolecules* **2015**, *48*, 8574–8584.

(33) Di, Z.; Posselt, D.; Smilgies, D. M.; Papadakis, C. M. Structural rearrangements in a lamellar diblock copolymer thin film during treatment with saturated solvent vapor. *Macromolecules* **2010**, *43*, 418–427.

(34) Di, Z.; Posselt, D.; Smilgies, D. M.; Li, R.; Rauscher, M.; Potemkin, I. I.; Papadakis, C. M. Stepwise swelling of a thin film of lamellae-forming poly(styrene-b-butadiene) in cyclohexane vapor. *Macromolecules* **2012**, *45*, 5185–5195.

(35) Bailey, T. S.; Pham, H. D.; Bates, F. S. Morphological Behavior Bridging the Symmetric AB and ABC States in the Poly(styrene-b-isoprene-b-ethylene oxide) Triblock Copolymer System. *Macromolecules* **2001**, *34*, 6994–7008.

(36) Bailey, T. S.; Hardy, C. M.; Epps, T. H.; Bates, F. S. A noncubic triply periodic network morphology in poly (isoprene-b-styrene-b-ethylene oxide) triblock copolymers. *Macromolecules* **2002**, *35*, 7007–7017.

(37) Jiang, Z. *GIXSGUI*: a MATLAB toolbox for grazing-incidence X-ray scattering data visualization and reduction, and indexing of buried three-dimensional periodic nanostructured films. *J. Appl. Crystallogr.* **2015**, *48*, 917–926.

(38) Ilavsky, J. *Nika*: software for two-dimensional data reduction. *J. Appl. Crystallogr.* **2012**, *45*, 324–328.

(39) Lee, B.; Park, I.; Yoon, J.; Park, S.; Kim, J.; Kim, K.-W.; Chang, T.; Ree, M. Structural Analysis of Block Copolymer Thin Films with Grazing Incidence Small-Angle X-ray Scattering. *Macromolecules* **2005**, *38*, 4311–4323.

(40) Smilgies, D.-M. Scherrer grain-size analysis adapted to grazing-incidence scattering with area detectors. *Journal of Applied Crystallography* **2009**, *42*, 1030–1034.

(41) Bates, F. S.; Fredrickson, G. H. Block copolymer thermodynamics: theory and experiment. *Annu. Rev. Phys. Chem.* **1990**, *41*, 525–557.

(42) Chatterjee, J.; Jain, S.; Bates, F. S. Comprehensive Phase Behavior of Poly (isoprene-b-styrene-b-ethylene oxide) Triblock Copolymers. *Macromolecules* **2007**, *40*, 2882–2896.

(43) Salvatore, S.; Demetriadou, A.; Vignolini, S.; Oh, S. S.; Wuestner, S.; Yufa, N. A.; Stefik, M.; Wiesner, U.; Baumberg, J. J.; Hess, O.; Steiner, U. Tunable 3D Extended Self-Assembled Gold Metamaterials with Enhanced Light Transmission. *Adv. Mater.* **2013**, *25*, 2713–2716.

(44) Dolan, J. A.; Wilts, B. D.; Vignolini, S.; Baumberg, J.; Steiner, U. Optical properties of gyroid structured materials: from photonic crystals to metamaterials. *Adv. Opt. Mater.* **2015**, *3*, 12–32.

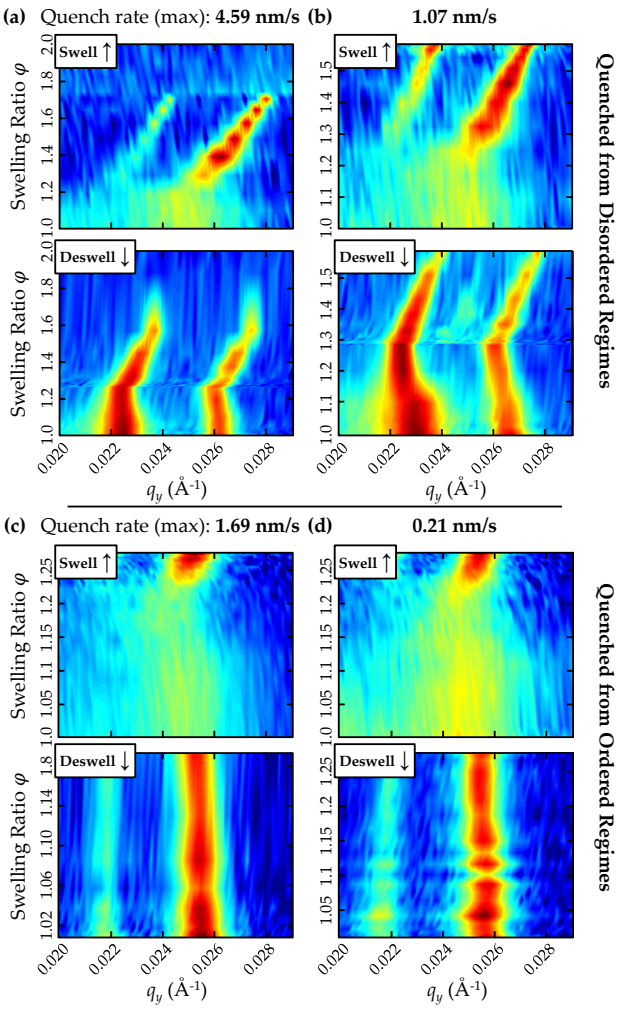

Figure S1: **Line integral surfaces of ISO thin films quenched from disordered and ordered regimes at different quench rates.** Swelling and deswelling line integral surfaces for ISO thin films which were in (a) and (b) disordered, and (c) and (d) ordered, regimes prior to quenching. Films were annealed in mixed vapors of THF and methanol (80:20). The films quenched from the disordered regimes exhibited a maximum solvent removal (quench) rate of (a) 4.59 nm/s and (b) 1.07 nm/s. The films quenched from the order regimes exhibited a maximum quench rate of (c) 0.21 nm/s and (d) 1.69 nm/s. The line integral surfaces plot the evolution as a function of swelling ratio of the line integral of the GISAXS pattern at the out-of-plane wave vector q_z corresponding to that of the $[1\bar{1}0]$ peak (cf. Figure 1). Logarithmic color scales are normalized to the maximum and minimum intensities of the complete set of line integrals.

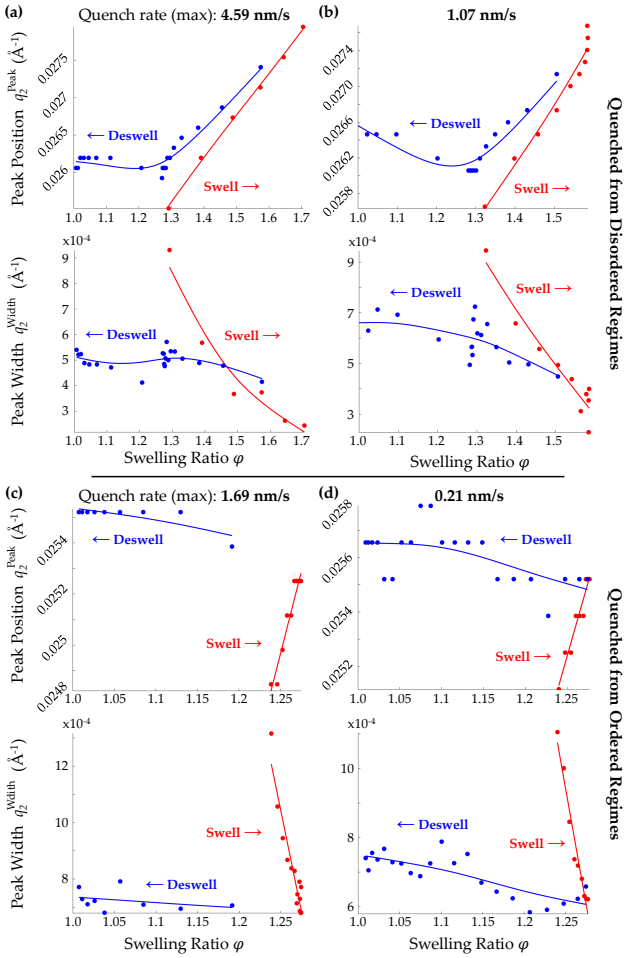

Figure S2: **Peak positions and widths during swelling and deswelling of ISO thin films quenched from disordered and ordered regimes at different quench rates.** Peak positions and widths during swelling and deswelling in mixed vapors of THF and methanol (80:20) of four ISO thin films. Peak metrics are calculated from the GISAXS line integrals. Peak positions and widths (i.e. full widths at half maximum) of the peak at the in-plane wave vector $q_y \approx 0.026\,\text{Å}^{-1}$ during swelling (red) and deswelling (blue) for films which are quenched from (a) and (b) disordered, and (c) and (d) ordered, regimes. The films quenched from the disordered regimes exhibited a maximum solvent removal (quench) rate of (a) 4.59 nm/s and (b) 1.07 nm/s. The films quenched from the order regimes exhibited a maximum quench rate of (c) 0.21 nm/s and (d) 1.69 nm/s. Solid lines are guides to the eye.

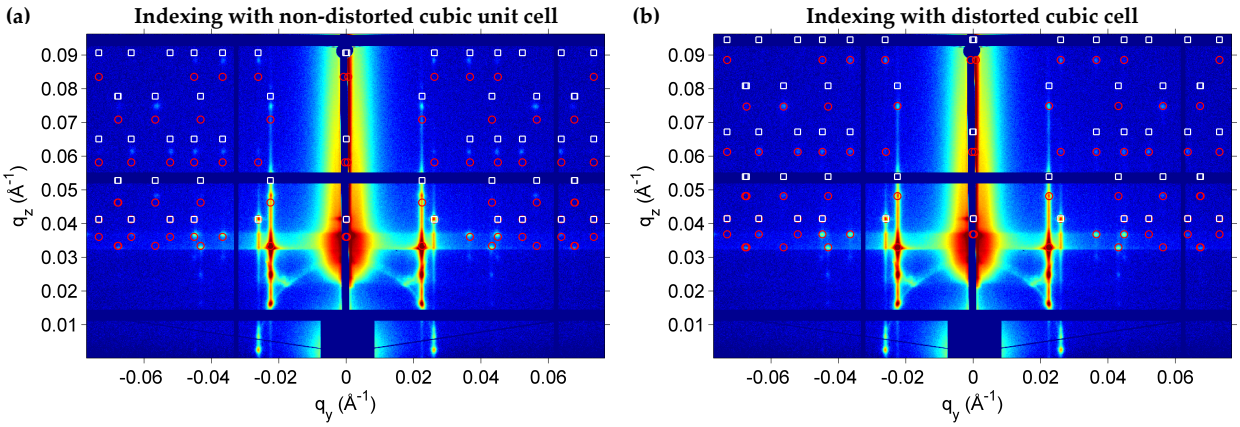

Figure S3: **Out-of-plane distortion in thermally annealed ISO2 films.** Indexed GISAXS patterns of an ISO2 film after annealing at 160°C for 1 h and subsequent quenching. Both patterns were indexed with peaks $(h, k, l = -4{:}4)$ of the $I4_132$ space group with the [110] direction oriented perpendicular to the substrate using the following unit cell paramaters (a) $a = b = 34.0\,\text{nm}$, $c = 34.2\,\text{nm}$, and $\gamma = 90°$, and (b) $a = b = 33.0\,\text{nm}$, $c = 34.4\,\text{nm}$, and $\gamma = 94°$.

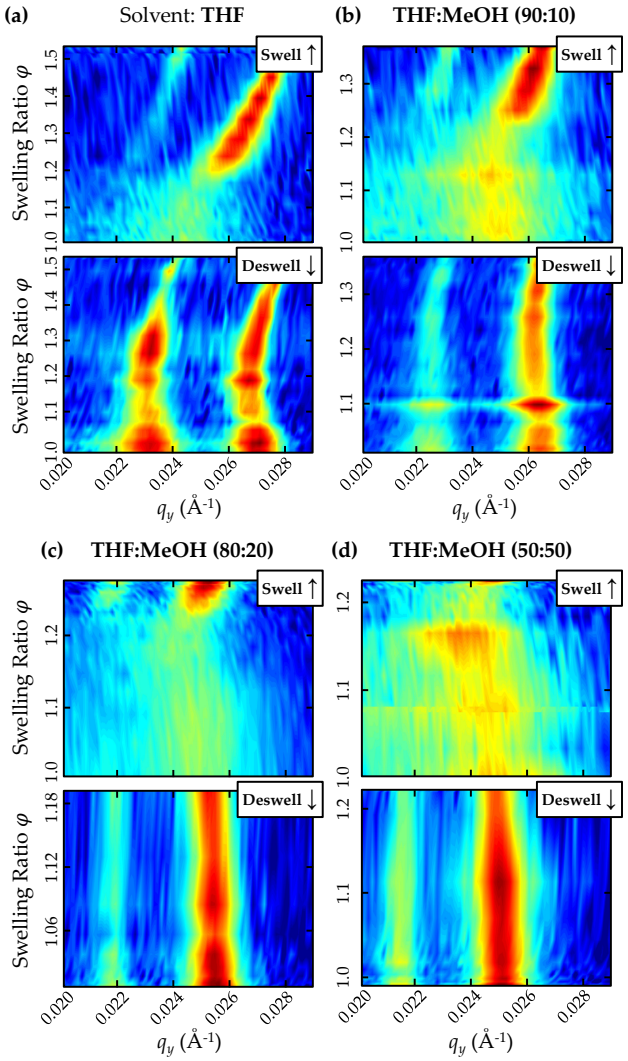

Figure S4: **Line integral surfaces of ISO thin films annealed in different compositions of solvent vapors.** Swelling and deswelling line integral surfaces for ISO thin films which were annealed in the vapors of (a) THF, (b) a mixture of THF and methanol (THF:MeOH) (90:10), (c) THF:MeOH (80:20) and (d) THF:MeOH (50:50). The line integral surfaces plot the evolution as a function of swelling ratio of the line integral of the GISAXS pattern at the out-of-plane wave vector q_z corresponding to that of the $[1\bar{1}0]$ peak (cf. Figure 1). Logarithmic color scales are normalized to the maximum and minimum intensities of the complete set of line integrals.